Biosensors based on carbon nanotubes and carbon nano-rings: A DFT study

Seyyed Mostafa Monavari
Semnan University
Farah Marsusi (marsusi@aut.ac.ir)
Amirkabir University of Technology
Nafiseh Memarian
Semnan University
Mohammad Qasemnazhand
Amirkabir University of Technology

Article

Keywords: density functional theory, glycoprotein, carbon nanoring, carbon nanotube, sequencing

Posted Date: August 1st, 2022

DOI: https://doi.org/10.21203/rs.3.rs-1863167/v1

Biosensors based on carbon nanotubes and carbon nano-rings: A DFT study

Seyyed Mostafa Monavari[1], Farah Marsusi[2,*], Nafiseh Memarian[1], Mohammad Qasemnazhand[2]

[1]Faculty of Physics, Semnan University, P.O. Box: 35195-363, Semnan, Iran

[2]Amirkabir University of Technology, P.O. Box 15875-4413, Tehran, Iran

Email: marsusi@aut.ac.ir

Abstract

We investigate the effect of glycoproteins on the optical properties of carbon nanotubes (CNTs) and carbon nanorings (CRNs), using density functional theory (DFT). Long rang correlation interactions are added by introducing van der Waals interaction. Our results show that the electronic and optical properties of both these materials are influenced by glycoprotein, which depends on their chirality and size. DFT can be used to predict the desired chirality and size of these nanomaterials. According to our outcomes, the predicted CNTs and CRNs may be chosen as the best sensitive and suitable candidates to use as bio-sensor materials.

Keywords: density functional theory**,** glycoprotein**,** carbon nanoring**,** carbon nanotube**,** sequencing**.**

1- Introduction

Due to the emergence of electronic devices and the significant changes in this field in recent decades, there is a need to build more accurate, smaller, and more capable sensors for environmental monitoring. Nowadays used sensors are sensitive to small amounts of any gas, heat, or radiation, however, still increasing the sensitivity, efficiency, and accuracy of these sensors is highly demanded. With the advent of nanoscience, dramatic changes have taken place in sensor technology. The combination of nanotechnology and medical sciences causes unprecedented achievements in developing new therapeutic and diagnostic methods. Biosensors could be classified based on the type of transmission mechanism. The most common classifications are electrochemical, optical, and field-effect sensors [1].

Single wall CNTs (SWCNTs) emit light when excited in the near-infrared range. When combined with specific polymers, they can be used as optical sensors for a wide range of analytes, including reactive oxygen species, insulin, dopamine, and nitric oxide (NO). These sensors react to the specific analyte, and this reaction manifests in the intensity of the fluorescence, thereby causing red and blue shifts in wavelength changes. Researchers are interested in developing SWCNTs as sensors for biological applications since the emission wavelengths of SWCNTs are close to the infrared range, in which water and blood have limited interference [2]. In addition, SWCNTs can be a good alternative to ITO in the coating layer due to their excellent optical properties, chemical stability, availability, the abundance of the carbon element, and high adhesion to different substrates [3]. The optical behaviours of these materials strongly depend on the chirality and geometry of the nanotubes (i.e., whether they are semiconductors or metals) [3]. In addition, CNTs are inherently fluorescent in the near-infrared region. A sensor could be operated by sensitizing nanotubes and observing the changes created in the absorption spectra in the presence of biomolecules. CNTs also have emissions in the near-infrared region, an area in which water and blood have limited interference, and they do not photo-bleach, therefore providing a long-term fluorescence sensor [4–7].

Recently, SEO et al. developed field-effect transistors (FETs) for a sensor device used in the clinical diagnosis of the COVID-19 virus. The sensor was evaluated by graphene sheets mixed with antibodies to measure its function against the COVID-19 virus molecule. Studies of the spike-binding of the virus protein to the graphene mixed with antibody showed doping-like changes on the graphene surface, while the sensor did not react to the MERS-Cov2 antigen. As such, a highly sensitive diagnostic tool should introduce against coronavirus [8].

In a study done by Wenting Shao, a biosensor consisting of high-purity semiconductor CNTs based on FETs was used to detect the COVID-19 virus, along with two types of biosensors, which were a nucleocapsid antigen (NAg) biosensor and a spike activated antigen (SAg) biosensor. Both biosensors showed very high sensitivity to the presence of the virus antigen. Clinical specimens are also used in designed biosensors without the need for laboratory preparation and processing, and the detection time in this method is significantly shorter than other test methods (approximately 5 minutes). Another advantage of CNT-based biosensors is their low cost. In the mentioned study, the detection limit of the device has been calculated to be 0.016 fg/ml for the nucleocapsid antigen and 0.55 fg/ml for the spike antigen. Furthermore, the obtained results indicated that devices with the spike protein antibody (SAb) function performed better in the

positive detection of the virus compared to the devices with the nucleocapsid protein antibody (NAb) function. In addition, the semiconducting single-walled carbon nanotube (SWCNT)-based field-effect transistor (FET) detection assay method provides the opportunity for the detection of multiple viral antigens, as well as the antibodies that detect these antigens [9].

To date, CNTs have been used in drug delivery nanosystems to battle against various viruses. In the most recent studies, the interaction between various types of multi-walled CNTs with different chirality's using the chemical vapour deposition method, against the SARS virus has been investigated and this technology could be applied for the preparation and manufacturing of diagnostic kits and protective medical devices [10]. Achieving diagnostic, inactivating, and virus-killing levels are critical today. In recent studies, SWCNTs with metal alloys have also been proposed as sensor substrate materials based on the density functional theory (DFT) [11].

CNTs are more reactive at the edges than other areas where the carbon atoms have dangling bonds. The reactivity of the side walls of the nanotube could be attributed to its structural properties and chirality [12]. Luong et al. reported that when CNTs are sonicated in organic solvents, they produce dangling bonds that are subjected to more chemical reactions [13].

The present study aimed initially to investigate the change in electronic properties of CNTs and carbon nano-rings (CNRs) in the presence of the glycoprotein molecule, using density functional theory (DFT). CNRs are observed in SWCNTs laser vaporization grew process [14]. For this purpose, we built zigzag, armchair, and general CNTs structures with chirality that allowed computational capabilities. Band structure, electron density of state (DOS), and energy gap are among the most important subjects are discussed in the field of sensors. The goal is analyzing the effectiveness of using CNTs and CNRs for the environmental monitoring of N-Link and O-Link glycoproteins. We have selected one case from each type of nanotube and investigated the electronic properties and energy gap of CNTs and energy levels of the highest occupied orbitals (HOMO) and the lowest unoccupied orbitals (LUMO) of CNRs, binding energy, chemical potential, ionization potential, electron affinity, chemical hardness/softness, and electronegativity in the presence of glycoprotein molecule. The binding energy of N-Link and O-Link glycoproteins is an important factor in sensing procedure. We also used time-dependent density functional theory (TDDFT) to calculate the absorption spectra of a CNR sample and monitored the change in its spectrum after being introduced to N-Link and O-Link glycoproteins. Our results show that with the presence of the N-Link and O-Link

glycoprotein molecules, the energy gap of the CNTs and CNRs may be changed and therefore they can be used for monitoring Corona-like virus spikes. Outcomes enable us to predict those structures that may show more sensitive optical and electronic responses in sensing devices, while our results can be detected experimentally through signals given by the built-in electronic device in biosensors.

2- Results

2-1-1 Armchair CNTs:

In this section, we will study the possible changes in the electronic properties of armchair (*n, n*) CNTs exposed to glycoprotein molecules. The diameter of the CNT is an important parameter helping us in finding the right case. Considering the computational cost, we have selected three types of armchair CNTs with chirality (2, 2), (3, 3) and (4, 4) and computed the corresponding electronic structure. As we expected and according to the prediction of a metal CNT when n-m=3|, we found that independent of the tube diameter, all three CNTs are metal. Some of the DFT-predicted structural and electronic properties of the nanotubes are given in Table 1.

Carbon nanotube	Electronic property	diameter (A)	Number of atoms	Chirality	Band gap (eV)	Other work band gap (eV)
(2, 2)	Metallic	2.91	24	Armchair	M2	Metallic[15]
(3, 3)	Metallic	4.39	36	Armchair	M2	Metallic[16]
(4, 4)	Metallic	5.53	48	Armchair	M2	Metallic[15]

Table 1. Properties of pristine CNT data that were used in calculations and the corresponding results.

The results presented in Table1 indicate good agreement with the previous data. We present the corresponding band structures in Figure 1, while the bands are extended from point Γ to the BZ boundary point at Z. Valence and conduction bands are represented by red and blue colours, respectively, in each figure.

M2 type mesh

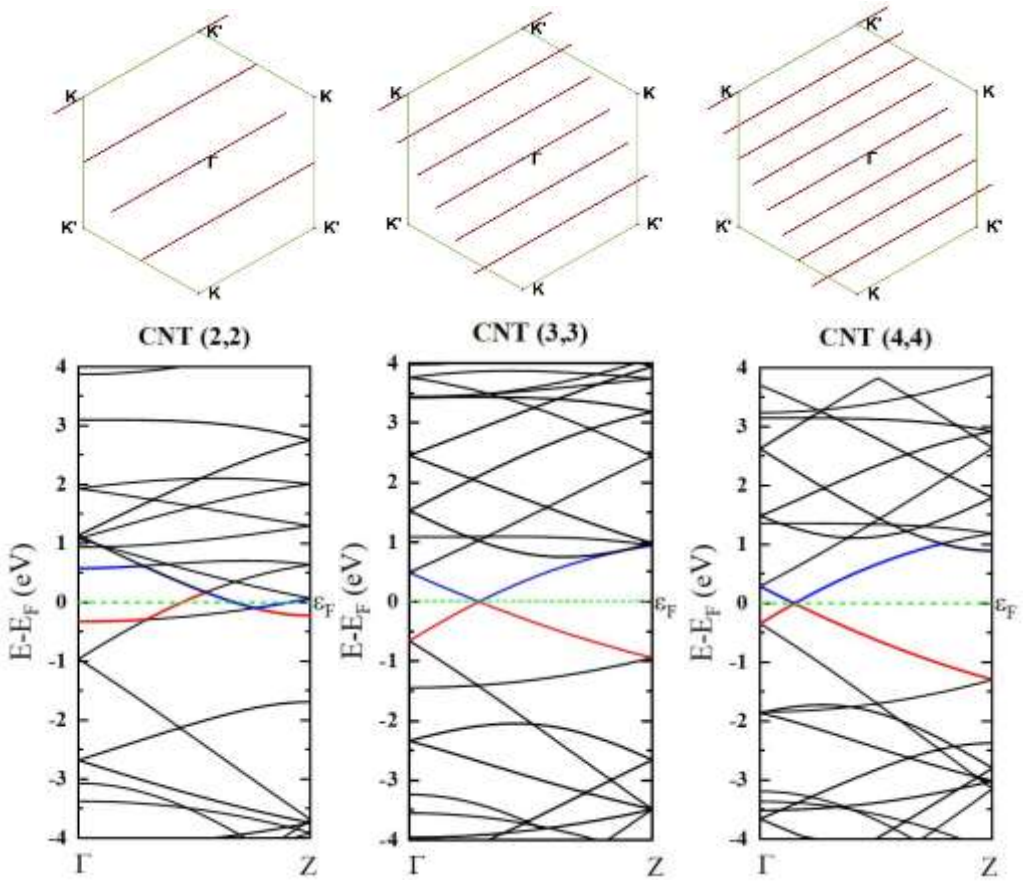

Figure 1 Top: Cutting lines in (BZ), bottom: the corresponding band structure diagram for (2, 2), (3, 3), (4, 4) armchair CNTs. The Fermi energy is set to zero.

Figure 2 shows that cutting lines cross the first BZ of "Armchair" CNTs at K and K′ and these nanotubes exhibit M2 metallic behaviors. [17-20].

2-1-2 Zigzag CNTs:

We selected four zigzag CNTs with chirality (3, 0), (4, 0), (5, 0) and (8, 0). Results are given in Table 2 and Figure 2, respectively.

Carbon nanotube	Electronic property	Diameter (A)	Number of atoms	Chirality	Band gap (eV)	Other work (eV)
(3, 0)	Metallic	2.69	24	Zigzag	M1	Metallic [15,20]
(4, 0)	Metallic	3.37	32	Zigzag	M	Metallic [16]
(5, 0)	Metallic	4.10	40	Zigzag	M	Metallic [15]
(8, 0)	Semiconductor	6.36	32	Zigzag	S2-0.598	0.571[21] 0.664[22]

Table 2. Properties of pristine CNT data. Results are compared with previous data taken from Ref. [15,16]， [20-22].

As expected, Table 2 shows that chirality has a significant influence on the electronic properties of zigzag CNTs. Zigzag CNTs with chirality of (3, 0), (4, 0) and (5, 0) are metals, while (8, 0) is a semiconductor with band gap of 0.598 eV.

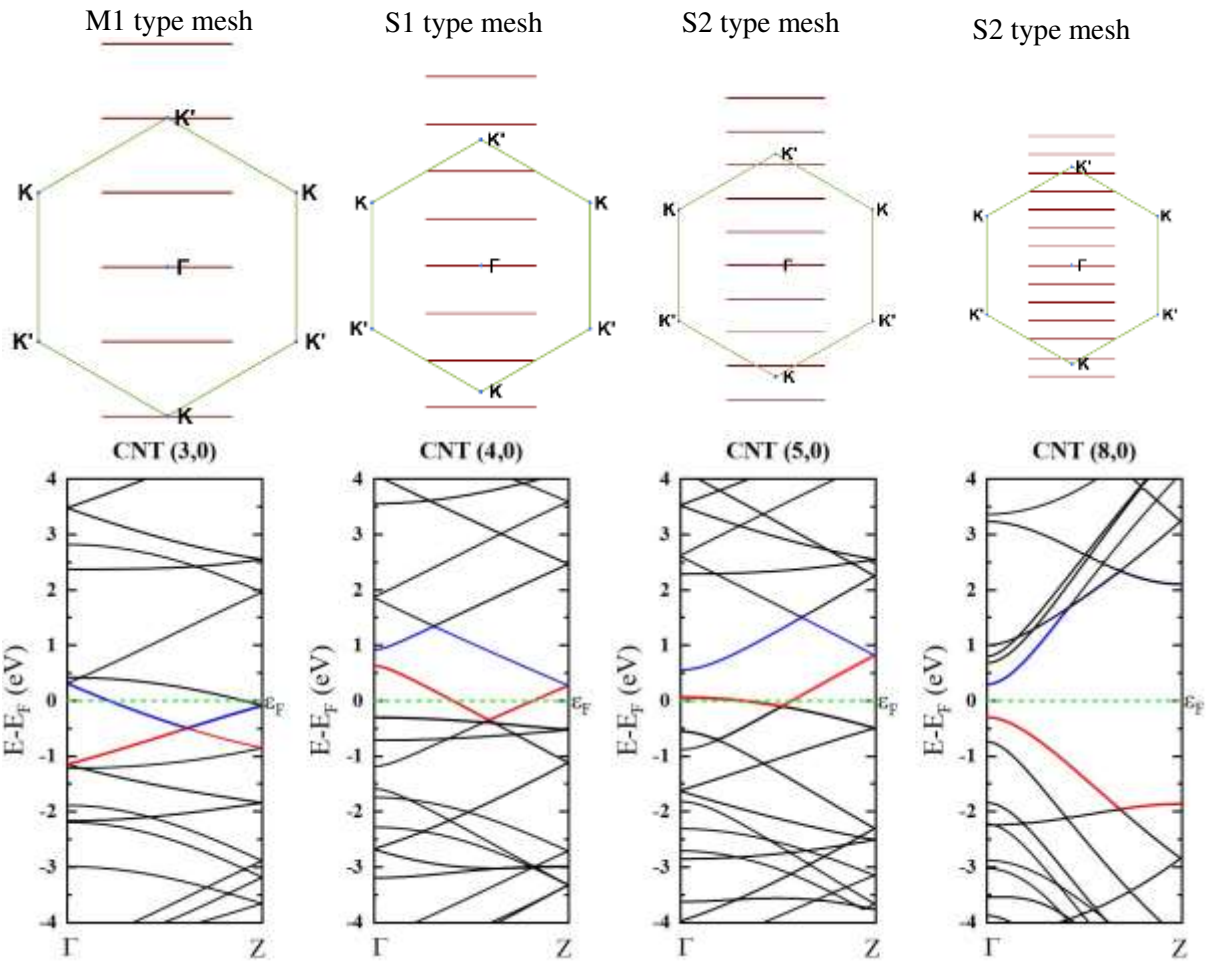

Figure 2. Cutting lines in (BZ) and band structure diagram for zigzag CNTs. According to the cutting line analysis shown in this figure, CNTs (4, 0) and (5, 0) should be semiconductor type S1 and S2, respectively, however, the structure curvature in these small tubes induces σ-π surface hybridization, and therefore metallic features, as concluded from the corresponding band structure.

Our results show that for CNTs (3, 0), the electron states (cutting lines) cross separately the (K, K′) points and the nanotube is M1-metalic type. Despite the metallic feature concluded from the calculated band structure shown in Figure 2, the small diameter of (4, 0) and (5, 0) CNTs induces σ-π hybridization effects to arise from the large curvature of the graphene folded layer and thereby causing an inaccurate prediction of semiconductor feature for these CNTs by of zone-folding scheme.

2-1-3 Chiral CNTs:

We have selected chiral CNTs (3, 1), (3, 2), (4, 1) and (4, 2) and investigated their energy gap, band structure and cutting lines. Results are shown in Table 3 and Figure 3 and compared with the previous data.

CNT	Electronic property	diameter (Å)	Number of atoms	Chirality	Band gap (eV)	Other work band gap (eV)
(3, 1)	Semiconductor	3.97	52	Chiral	S2-0.705	0.720[15]
(3, 2)	Semiconductor	3.60	76	Chiral	S2-0.360	0.310[15]
(4, 1)	Metallic	3.74	28	Chiral	M1	Metallic[17-18]
(4, 2)	Semiconductor	4.28	56	Chiral	S2-0.233	0.190[15,19]

Table 3. Properties of pristine CNT data.

DFT predicts that the geometric structure imposes metallic feature to CNT (4, 1). The other CNTs are predicted semiconductors, while the largest electronic band gap of 0.705 eV for CNT (3, 1) and the lowest energy gap of 0.233 eV is predicted for CNT (4, 2).

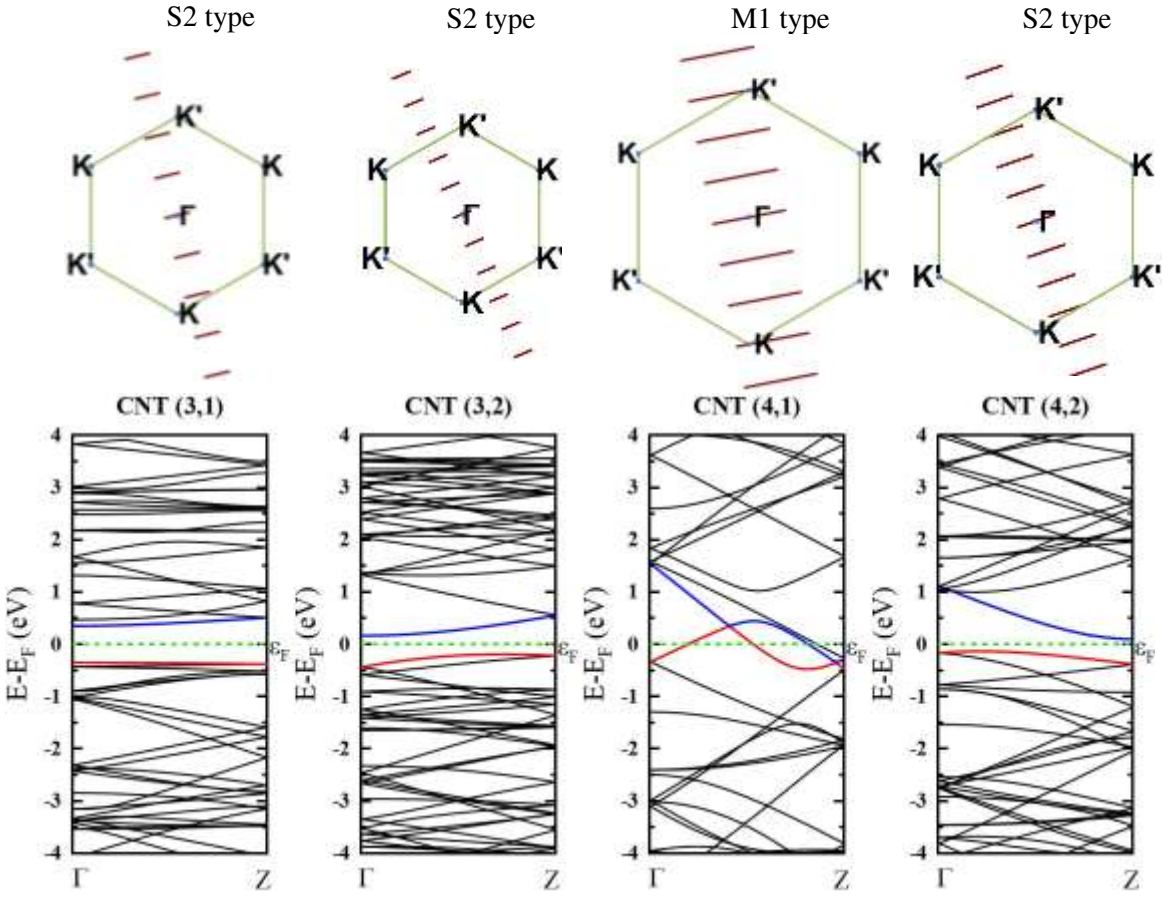

Figure 3. Cutting lines in (BZ) and band structure diagram for chiral CNTs. According to both the cutting line analysis and band structure feature, the three (3, 1), (3, 2), (4, 2) CNTs are semiconductors, while CNT (4, 1) is metal.

For CNT (4, 1), there always exist two electronic states that cross the K and K′ points in (BZ) Separately, and therefore these nanotubes always show an M1-metallic behavior. While for other nanotubes no electronic states pass the points K, K′ and are S2-semiconductors.

2-2 Single-walled CNTs next to glycoprotein molecules

Virus spikes often contain glycoproteins. Glycoproteins are composed of carbohydrates and proteins and have several different types. Two main sections in the Corona-virus spikes are the N-Link and O-Link glycoproteins. The naming of these two types of glycoproteins relates to the atomic type that binds the protein moiety to the carbohydrate moiety. If this bond includes an oxygen atom, the glycoprotein is called the O-Link type, and if it contains a nitrogen atom, the glycoprotein is called the N-Link type. Figure 4 illustrates the optimized structure of these two types of glycoproteins [23].

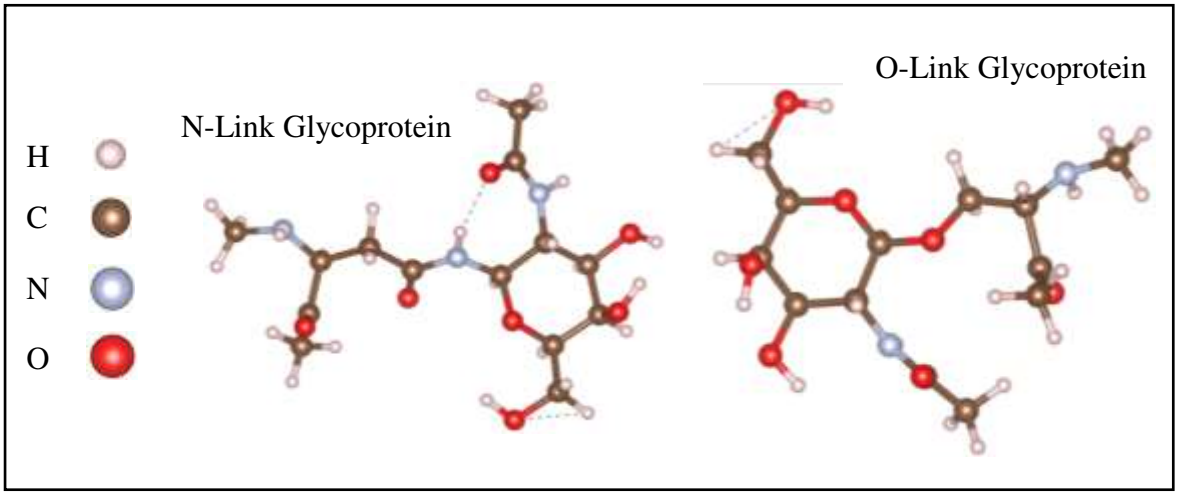

Figure 4. Common glycoproteins in corona-virus spikes (N-Link and O-Link).

In the following, we investigate the effect of adding glycoprotein to a CNT with metallic and semiconductor electronic features. For this purpose, two types of chiral CNT (3, 1) and CNT (4, 2) and a zigzag CNT (4, 0) and CNT (3, 3) M2 type were selected.

We placed the N-link and O-link glycoprotein molecules in a unit cell perpendicular to the CNTs. After optimization, the molecules moved to the edges of the CNTs. The effect of the presence of glycoprotein molecules on the energy gap of the selected CNTs is reported in Table 4. The change in the electronic gap of the composing structure compared to the pristine CNT was calculated from Equation 1.

$$\Delta E_{gap} = E_{gap}\left(\text{Glycoprotein} - \text{CNT}\right) - E_{gap}\left(\text{CNT}\right), \quad (1)$$

Where ΔE_{gap} is the *change* in the band gap energy of the CNT after the presence of the glycoprotein-containing, E_{gap} (glycoprotein-CNT) is the band gap of CNT in the presence

of the glycoprotein and E_{gap} (CNT) is the band gap of the pure CNT. Table 4 lists data corresponding to the structure of glycoproteins-containing CNT, number of atoms in the unit cell, chirality, band gap energy and $\Delta E_{gap,}$ respectively.

Structure	Number of atoms	Chirality	Band gap (eV)	ΔE_{gap} (meV)
N-Link (3, 3)	85	Armchair	M	M
O-Link (3, 3)	82	Armchair	M	M
N-Link (4, 0)	81	Zigzag	M	M
O-Link (4, 0)	78	Zigzag	M	M
O-Link (3, 1)	98	Chiral	0.303	-402
O-Link (4, 2)	102	Chiral	0.227	-6

Table 4. The structure under study, the corresponding number of atoms in that structure, the chirality of the structure, the corresponding band gap, and the change in the band gap according to Equation. 1.

According to Table 4, the addition of glycoprotein molecules cannot change the electronic feature of metallic CNTs, as we see for (3, 3), and (4, 0) CNTs. However, for a semiconductor type the CNT (3, 1) by adding the O-link glycoprotein, the electronic gap reduces from 0.705 to 0.303 eV with a change of 402 meV, and a smaller reduction of 6 meV is observed, when for (4, 2) chiral CNT. Figure 5 illustrates the effect of the presence of glycoprotein on the band structure of the mentioned CNTs. By comparing the results shown in Figures 1-3, it could be inferred that the presence of N-Link and O-Link glycoproteins in the CNT medium can change the band structure and electronic gap of semiconductor CNTs. We further studied the selected CNTs in the presence of an O-link glycoprotein. Figure 6 depicts the electron density of the state diagram for glycoproteins in the presence of the selected CNTs. The Fermi energy is set to zero with a green dashed line.

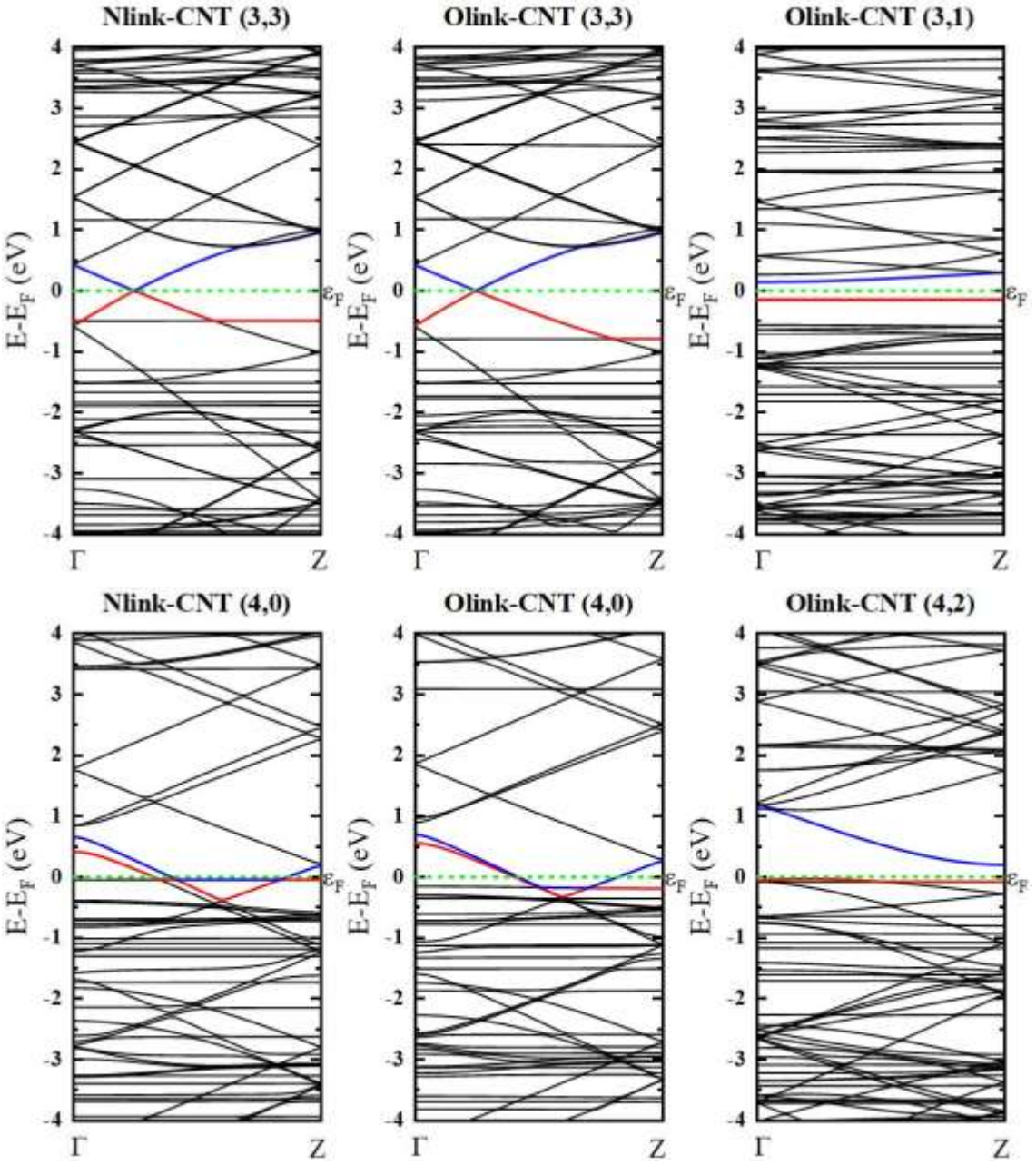

Figure 5. Band structure of selected CNTs given in Table 4 in presence of glycoprotein

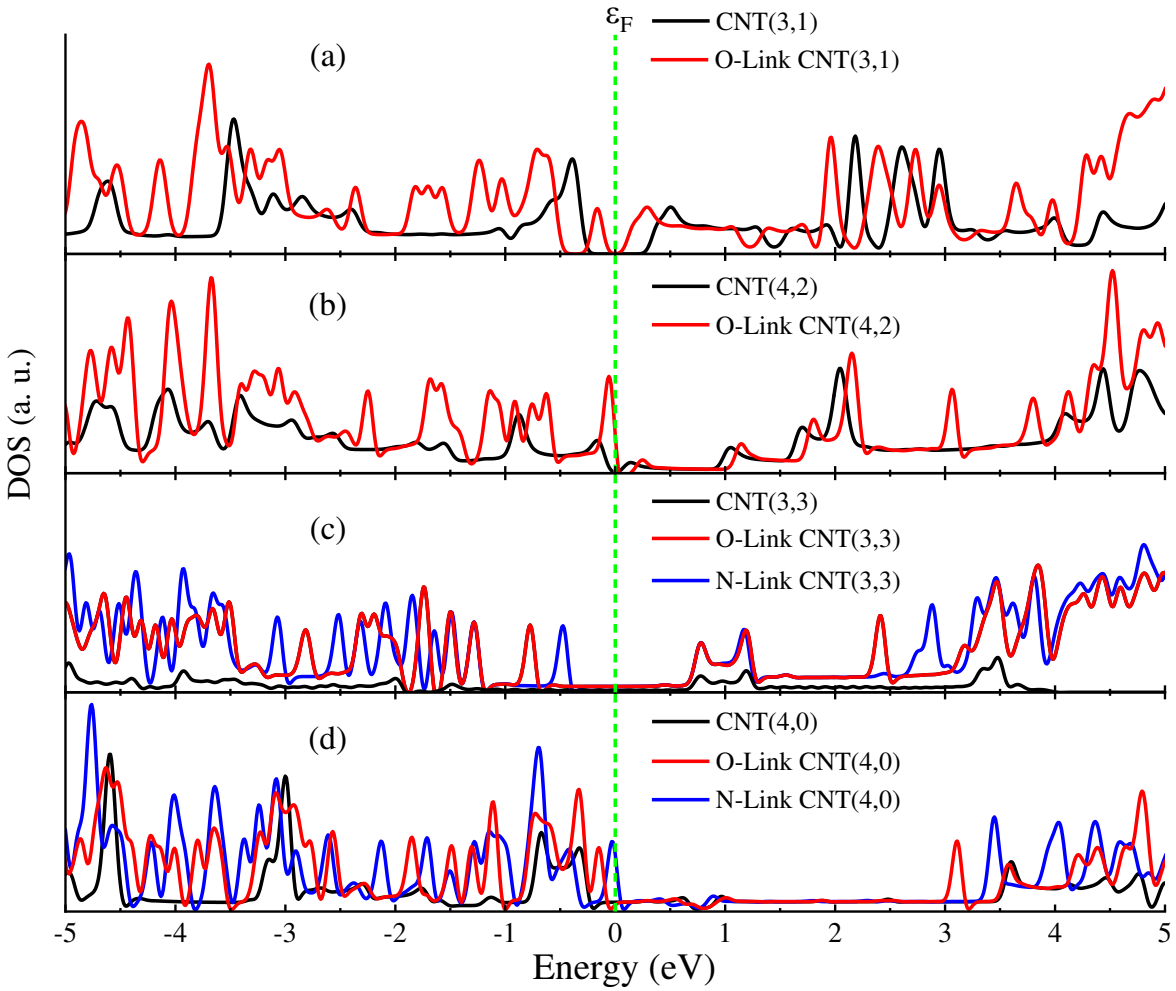

Figure 6. Diagram of Electron density of states for CNTs and N-link and O-link Glycoproteins.

Figure 6 compares the energy density of states in the presence of glycoproteins with the pure nanotubes. The obtained results indicated an increase in the density of the nanotube carriers due to the presence of glycoprotein molecules. However, the presence of glycoprotein in Figure 6-b did not show significant changes in the gap of the CNT (4, 2), and only the energy of the full and empty bands shifted to the right (higher energies). As it is depicted in Figures 6-c and 6-d, the Fermi energy cut the valence and conduction bands of CNTs (3, 3) and (4, 0), and the presence of electron density could be observed in these zones. So, we can say that semiconductor CNTs, like chiral (3, 1), may be proper candidates that can exhibit appropriate and predictable behavior.

2-3 Single-walled Carbon Nanoring and the Effect of the Glycoprotein

Armchair CNRs are effective models for the synthesis of CNTs. The length of the smallest armchair nanoring is related to cycloparaphenylene (CPP) [24], which was synthesized in 2008 and is about the width of a benzene ring. According to the findings of Omachi et al. [25], the chemical synthesis of CPP[*n*], in which [*n*] shows the number of

the benzene rings in the modular synthesis method, determines the size of the CNT produced from a CPP[n]. Therefore, the computational possibilities for identifying glycoproteins led us to select the CNR (8, 8) with a diameter of 1.22 Å. We also evaluated the effect of increasing the nanoring length on the detecting of N-Link and O-Link glycoprotein molecules by adding one armchair carbon layer to the CNR (8, 8) with L1 length. By this, the length of the CNR increased from $L_1 = 5.57\,\mathring{A}$ to $L_2 = 6.82\,\mathring{A}$. Figure 7 shows the optimized structure of CNR (8, 8) with lengths L_1 and L_2.

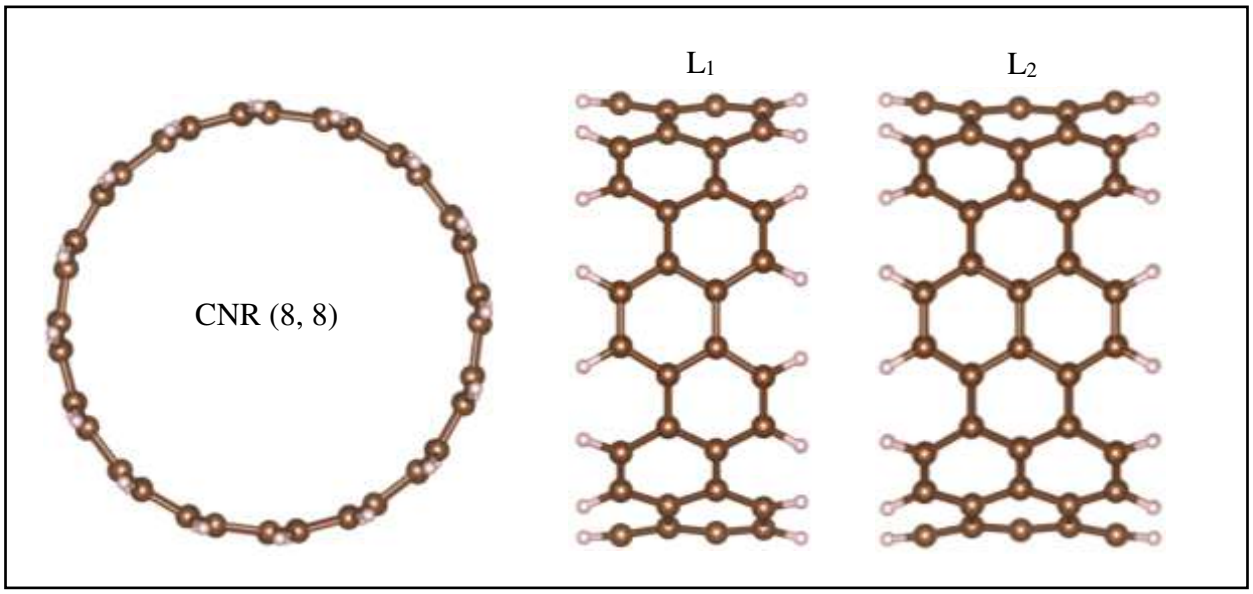

Figure 7. Cross-section and Lateral Surface of CNR (8, 8) with Lengths L1 and L2.

Due to the ability of covalent bonds to control the biomolecule location, the best conditions for stability, acceptability and selectivity are determined where the covalent bonds between CNRs and glycoproteins may be formed [13]. Results showed that glycoproteins form covalent bonds with CNRs, and surface hybridization of carbon atoms is changed from sp^2 to sp^3.

Another objective of the present study was to identify the indicators that could be used to make a sufficient distinction between glycoprotein molecules. These indicators were expressed in the form of electrochemical properties.

The main electronic properties included the energy of the HOMO and LUMO orbitals, the electron gap (E_{gap}), chemical potential (μ), electronegativity (χ), hardness (η), chemical softness (σ), electron affinity (EA), ionization potential (IP), binding energy (BE), and electron felicity (ω). These properties could be obtained using the following equations [24-30]:

$$\Delta E_{gap} = E_{LUMO} - E_{HOMO} \quad (2)$$

$$\mu = \frac{E_{HOMO}+E_{LUMO}}{2} \quad (3)$$

$$\chi = -\mu$$

$$\eta = (\frac{E_{HOMO} - E_{LUMO}}{2}) \quad (4)$$

$$\sigma=1/\eta \quad (5)$$

$$E_A = -E_{LUMO} \quad (6)$$

(7)

$$IP = -E_{HOMO} \quad (8)$$

Moreover, electron felicity was calculated based on the chemical potential and chemical hardness using Equation (9):

$$\omega = \frac{\mu^2}{\eta} \quad (9)$$

The most important factor considered in this section is the separation between binding energy of N-Link and O-Link glycoproteins by sensor substrate (CNRs). The binding energy has been defined using Equation (10).

$$\Delta E_B = E(CNR + Glyc.) - [E(CNR) + E(Glyc.)], \quad (10)$$

$E(CNR + Glyc.)$ shows the energy of the entire system of CNR and glycoproteins, $E(CNR)$ shows the energy of the individual CNR, and $E(Glyc.)$ represents the energy of the individual glycoprotein [31]. The results are displayed in table 5.

Structure	HOMO	LUMO	E_{gap}	μ	IP	EA	χ	η	σ	ω	ΔE_B

Glycoprotein											
N-link	-4.48	-1.56	2.93	-3.02	4.48	1.56	3.02	1.46	0.68	3.12	--
O-link	-4.90	-2.08	2.82	-3.49	4.90	2.08	3.49	1.41	0.71	4.32	--
Length Size1											
(8, 8)	-4.93	-2.54	2.39	-3.73	4.93	2.54	3.73	1.19	0.84	5.83	--
N.Glyc.+CNR(8, 8)	-4.37	-2.80	1.57	-3.58	4.37	2.80	3.58	0.78	1.28	8.20	-0.32
O.Glyc.+CNR(8, 8)	-4.65	-2.69	1.97	-3.67	4.65	2.69	3.67	0.98	1.02	6.85	-0.12
(N&O).Glyc.+CNR(8, 8)	-4.40	-2.90	1.50	-3.65	4.40	2.90	3.65	0.75	1.33	8.88	-0.60
Length Size2											
(8, 8)	-4.06	-3.35	0.72	-3.71	4.06	3.35	3.71	0.36	2.79	19.18	--
N.Glyc.+CNR(8, 8)	-4.32	-3.62	0.70	-3.97	4.32	3.62	3.97	0.35	2.87	22.56	-0.30
O.Glyc.+CNR(8, 8)	-4.18	-3.49	0.70	-3.84	4.18	3.49	3.84	0.35	2.87	21.10	-0.13

Table 5. A list of HOMO, LUMO, H-L Gap, chemical potential (μ), ionization potential (IP), electron affinity (EA) electronegativity (χ), chemical hardness (η), chemical softness (σ), electron felicity (ω) and the differences of binding energy (ΔE_B) for O and N-Link glycoproteins, CNR(8, 8) with two lengths of L1, L2 and their complex systems together (in unit eV).

Since a sensor material should be chemically stable, materials with a higher chemical hardness are more suitable for this purpose. According to the information in Table 4, the CNR with length L_1 is a better option for detecting molecules owing to better sensitivity, the larger change in the electronic gap in the presence of glycoprotein, and more stability (higher chemical hardness) than CRN with longer length L_2.

In Figure 8, we pictorially show the HOMO and LUMO energy changes in the presence of glycoprotein molecules.

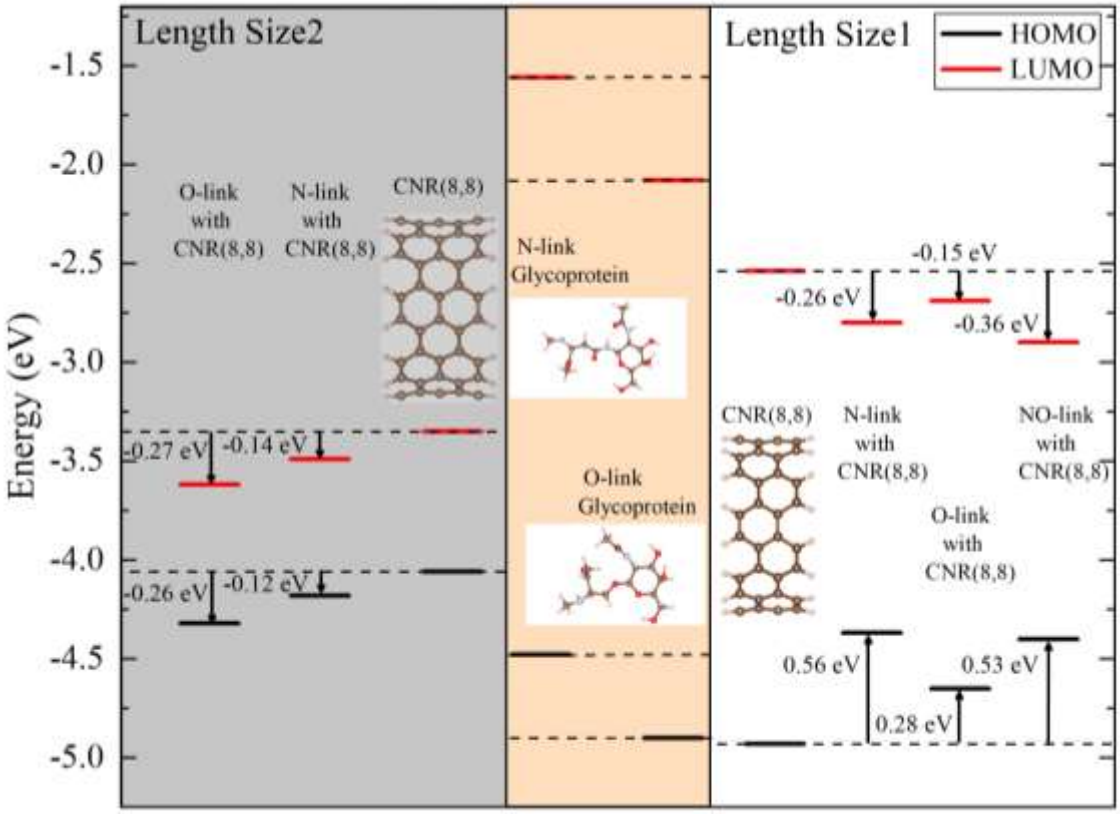

Figure 8. Changes in the HOMO and LUMO energy of CNTs (8, 8) in Lengths L1 and L2 due to the presence of glycoprotein molecules.

According to Figure 8, at L1 length, glycoprotein molecules increase HOMO energy levels and decrease LUMO energy levels for CRN (8, 8). Thus, the energy gap has undergone a serious change. However, at L2 size, glycoprotein molecules reduce both the HOMO and LUMO energy levels and no significant change happens in the energy gap. The van der Waals interactions between CNTs and glycoprotein molecules are greater for narrow lengths. Therefore, glycoprotein diagnostic devices based on L1 size CNR (8, 8) are better options.

Hydrogen bonding strength could be classified into three groups depending on the amount of energy. Strong bond energies are greater than 0.65 eV, moderate bond energies happen at 0.17 – 0.65 eV, and weak bonds for dependent energies are less than 0.17 eV [32,33]. The calculated binding energies are shown in Table 5, showing that the hydrogen bond strength for the carbon nanoring (8, 8) in the presence of the N-Link glycoprotein is moderate for both lengths. While this value is weak for carbon nanoring (8, 8) in the presence of O-Link glycoprotein .

In the following, we examined the ability of CNRs (8, 8) to determine whether they could sense the presence of a glycoprotein. The reaction of CNRs (8, 8) to the presence of the intended glycoproteins was investigated with possible changes in the electron density of state. Figure 9 illustrates the density of state diagrams for glycoproteins, single L1 size CNR (8, 8), and glycoprotein-nanoring composite systems.

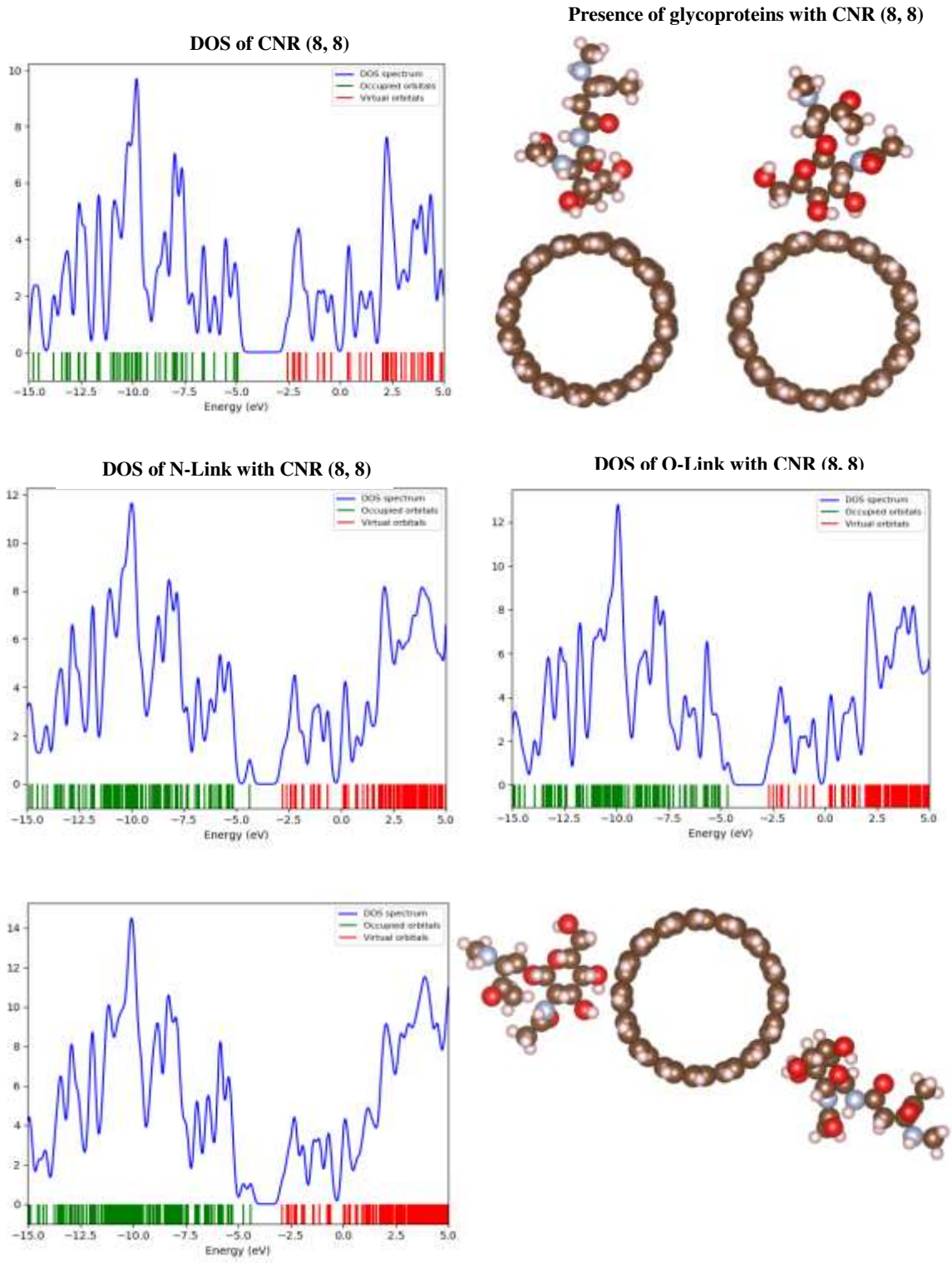

Figure 9. Electron density of states diagrams for L1 size CNRs (8, 8) in absence and presence of N-Link and O-Link glycoprotein molecules.

As clearly shown in Figure 9, the structures had a high electron affinity due to the negative LUMO levels. Moreover, the results show that the entry of glycoprotein molecule into the L1 size CNR (8, 8) reduces the LUMO level energy and increased the HOMO level. In this case, we see the most electron affinity and the most changes in the electron gap. Moreover, adding N-Link glycoprotein to the CNR (8, 8) led to a further decrease in the LUMO level and an increase in the HOMO level compared to O-Link. Therefore, the

electron density of states confirmed the detection and differentiation of glycoprotein molecules by the CNR (8, 8).

To investigate the changes in the HOMO and LUMO levels after adding the glycoprotein molecules to the CNR (8, 8), the HOMO and LUMO orbitals representation of the individual glycoproteins, CNR (8, 8), and CNR (8, 8)-glycoprotein composite systems are shown in Figure 10.

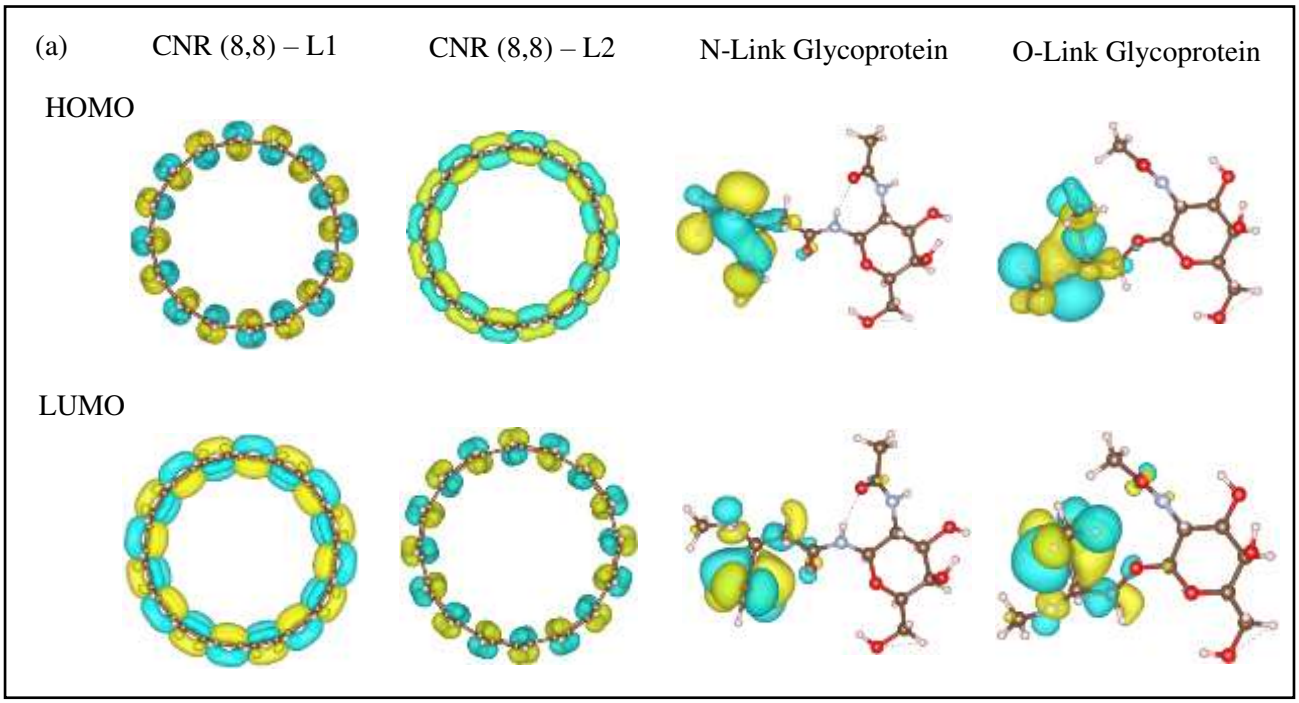

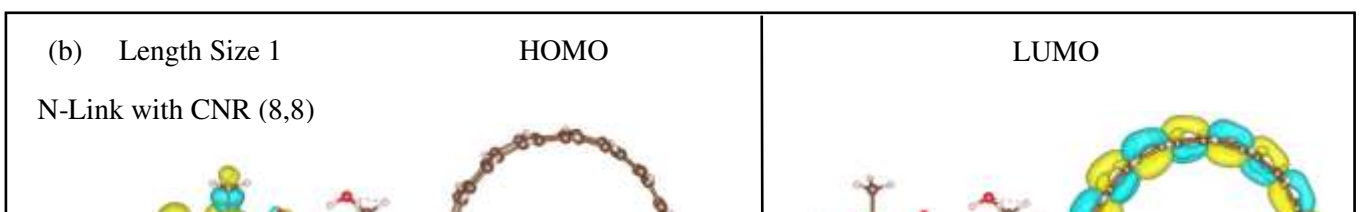

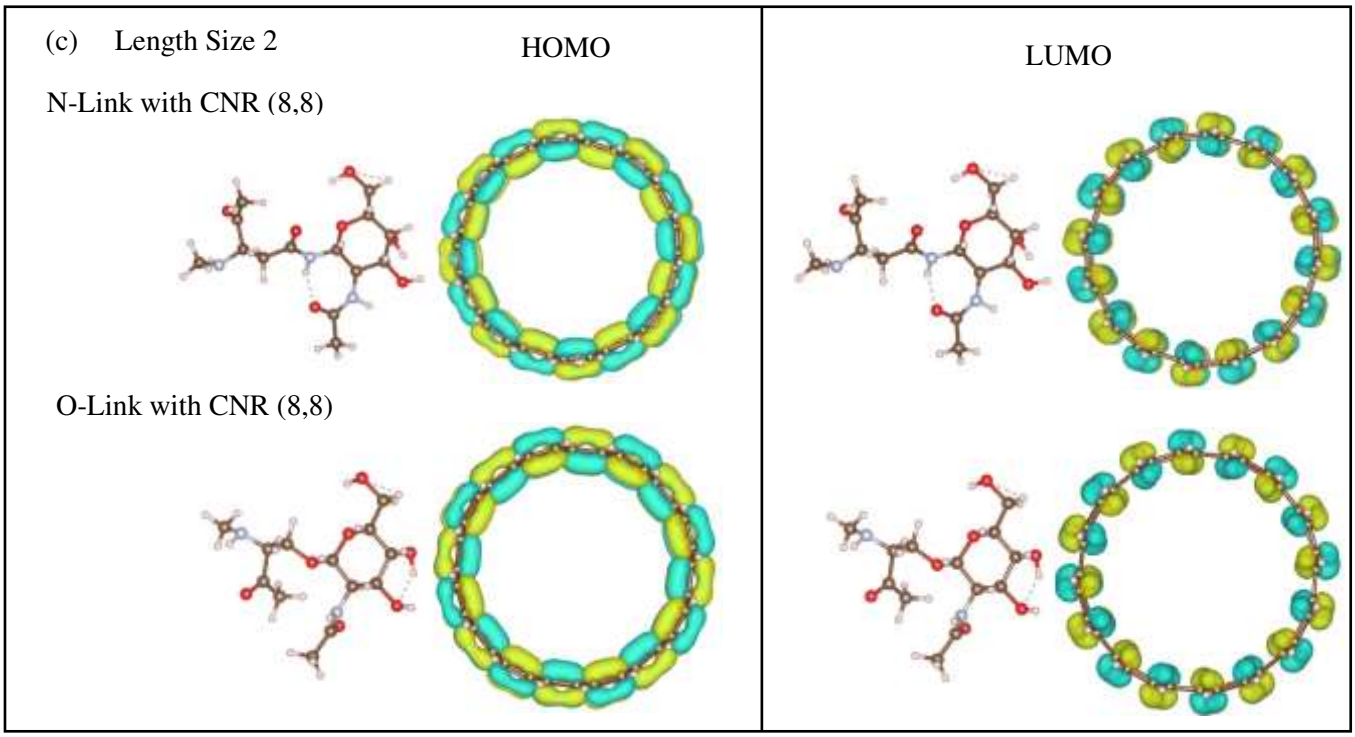

Figure 10. (a) HOMO and LUMO orbitals for pure CNRs (8,8) and glycoproteins. (b), (c) HOMO and LUMO orbitals for composite systems CNR (8,8) and glycoproteins in length size 1 and 2 respectively (Isovalue: 0.02).

The introduction of high electronegative factors such as oxygen, or nitrogen presented by glycoprotein molecules to the L1 size CNR (8, 8) caused intense changes in the electronic properties of L1 size CNR (8, 8). The HOMO surface shows a charge localization on the amino or ketonic functional group of the glycoprotein molecules so that N-link and O-link groups suppress the electronic dynamics of the combined structure through nonbonding electron pairs on the functional groups. That means the nonbonding pair of electrons in nitrogen and oxygen atoms dominate the HOMO state and imposes a

new level inside the HOMO-LUMO gap of pristine L1 size CNR (8, 8), as concluded from Figure 8. This finding is confirmed by the density of state diagrams in Figure 9 and the HOMO orbital representation in Figure 10. Also, the presence of oxygen increased the chemical potential of the structure, and the electron can more easily excite, or the structure can be ionized with less energy than before. As a result, changes in the electron density of state and the HOMO-LUMO orbital representation indicated differences in the properties associated with electronic behaviors (e.g., optical properties). One of the important optical properties that are applicable in biosensors is the electronic absorption spectrum. Thereby, we show how the absorption spectrum of a CNR (8, 8) with length L_1 changes due to the presence of the intended glycoproteins. TD-DFT predicted spectra of CNR (8, 8) in the presence of glycoprotein molecules are shown in Figure 11. Since B3LYP often predicts more realistic absorption spectra, owing to cancellation of localization and delocalization errors, we used B3LYP in addition to PBE functional in this section.

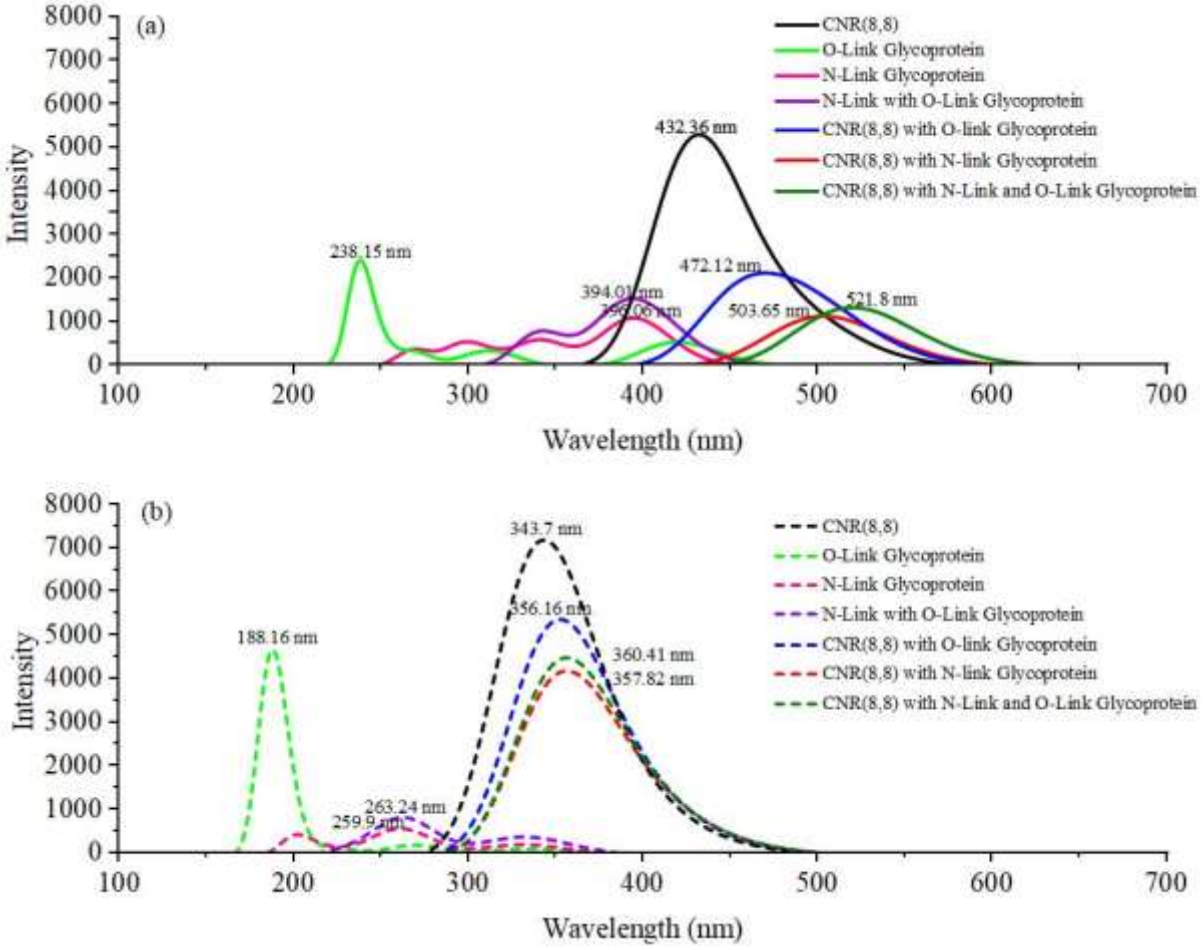

Figure 11. (a) PBE TD-DFT predicted absorption spectra, (b) B3LYP TD-DFT predicted absorption spectra. In both figures, as the glycoprotein approaches the CNR, the absorption spectra shift toward the visible region .

Both functionals show that the glycoprotein molecules have no physical absorption in the visible region, and the absorption of N-Link, O-Link, and N-Link with O-Link together is in the ultraviolet region [34]. Interestingly, when glycoproteins are present in the environment around the CNR (8, 8) with L1 length, the spectra of the complex system show redshifts shifts toward the visible region stemming from the Van der Waals interactions. These changes are more evident in Figure 11 (a).

The effect of the added glycoproteins on the intensity of the absorption was more significant in Figure 11 (b) compared to Figure 11 (a), while redshifts were observed in both cases. Adding of O-Link glycoprotein also changed the sample's colour from purple to blue. Also, changes in the colour of the sample were primarily associated with the case that both types of glycoproteins were added to the CNR. In this case, the colour of the sample changed from purple to light green. Results suggest that the distance between the oxygen portion of the protein fraction of the distance of the carbohydrate fraction of the glycoprotein from the surface of the CNR significantly affects the changes in the absorption spectrum as the presence of oxygen changes the electron density around the CNR. Therefore, it could be stated that CNR (8, 8) is a viable option for glycoprotein sequencing.

3- Discussion

In this study, we investigated the change in the electronic properties of several CNTs and selected CNRs in the presence of N-link and O-link glycoprotein molecules. Our results show that, depending on the size and chirality, the CNT or CNR can be a good option for use as biosensor materials. Specially we found, that depending on chirality and size, CNR can show appropriate electronic and optical sensitivity required for sensors. In the case of CNR (8, 8) the presence of these molecules, depending on the size of the CNR gives large optical alterations. The present study gives important findings in diagnosis materials for viral diseases based on CNTs. Given their biocompatibility, we concluded that, CNRs could be used in environmental health design.

4- Methods

4-1 Calculation Method of CNTs

In this section, we examine the mechanism for calculating the electronic properties of CNTs and the effect of adding glycoprotein molecules. Calculations were performed within the framework of the plane-wave pseudopotential DFT-PBE approach, using Quantum-Espresso computational package [35-36]. The effect of core ions was performed using the Perdeo-Berk-Ernzerhof pseudopotential. The Grimme's vdW correction (PBE-D2) is added to our calculations to introduce the long-range effect of van der Waals interactions to calculations. The simulation was performed at room temperature (300 K). The cutoff energy on the plane-wave basis was set to 45 Ha. A $1\times1\times12$ Monkhorst **k**-point mesh was used to sample the Brillouin zone (BZ) [37]. Moreover, the volume of the supercell and the atomic positions of the structures were optimized under conditions where the forces acting on atoms are less than 5 meV/A. Periodic boundary conditions along the growth direction have been applied to all structures.

4-2 symmetry-dependent electronic properties of CNT

The chirality (n, m) of CNTs shows the way that a graphene sheet is enfolded. We can show the structure of an SWCNT by taking two hexagons of a graphene sheet and rolling up the sheet to overlap the two hexagons. A vector that connects the center of two hexagons is named a chiral vector, as seen in Figure 12. Chiral vector is written in terms of the primitive vectors a_1 and a_2, of graphene lattice in the form of $C_h = n\,a_1 + m\,a_2$, and n and m are integer numbers. If n=m=|, where | is zero or any integer positive number, the resulting nanotube is called an armchair (n, n) CNT. A zigzag CNT (n, 0) is formed when n=| and m=0. Other combinations of n and m are called chiral CNT [38]. An SWCNT has metallic properties with zero electronic gaps, if n-m=3| [39], otherwise, the SWCNT behaves as a semiconductor with an electronic gap that depends on the chirality (n, m) and inversely proportions with CNT diameter [40]. Therefore, the geometry of CNT plays an important role in its electronic properties.

In the reciprocal space, the allowed states are called cutting lines. The chirality of the CNT determines the orientation of the cutting lines [41]. Depending on whether the cutting line crosses the degenerate K and K' points of BZ, an SWCNT behaves as either metallic (M), n-m=3|, or a semiconductor (S), n-m≠3| [42]. In a metallic CNT, the cutting line crosses the *K* point. Depending on what ratio the K point divides the cutting line, the metallic CNTs can be classified as M1 or M2. Following Ref. [42], we name the greatest

common divisor of the (2n+m, 2m+n) by d_R and of the two integers (n, m) by d. In M1 type CNT d_R=d, while in M2 type CNT d_R=3d.

On the other hand, CNT cutting lines do not crosse the K point in a semiconductor CNT and the *K* point could be located at either one-third (S1) or two-thirds (S2) of the distance between two adjacent cutting lines [42].

An armchair CNT (n, n) is always M2-type metallic. For a zigzag CNT three types are possible: an M1 (3|,0) or S1 type (3|+1) or S2 type (3|+2). For a chiral CNT each of the four types M1, M2, S1, and S2 is possible [42].

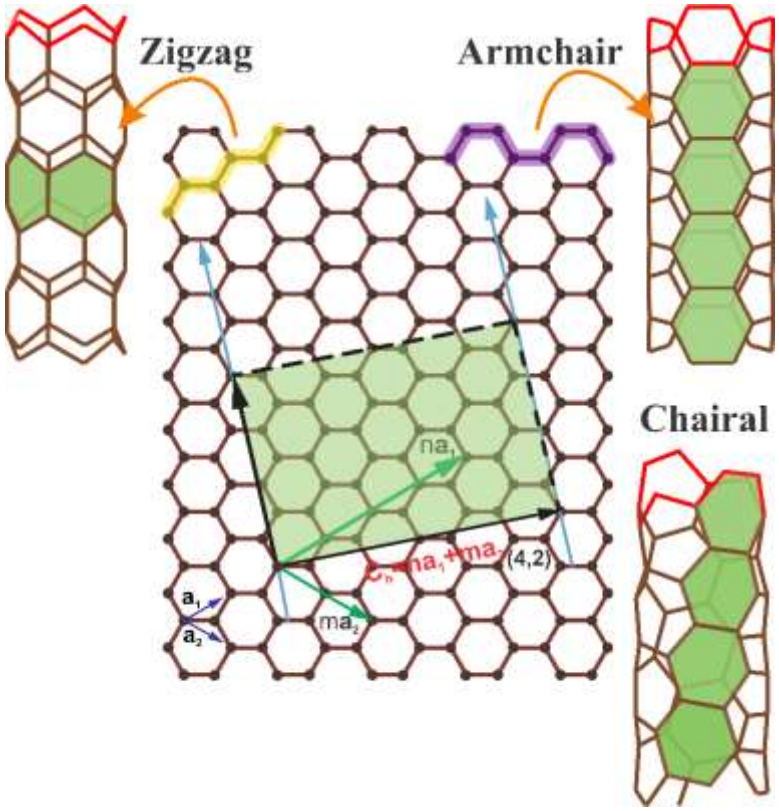

Figure 12: The structure of SWCNT can be shown by a graphene sheet when is wrapped along the chiral vector $C_h = n\,a_1 + m\,a_2$. a_1 and a_2 show the graphene primitive vectors with Illustration of three types of CNT.

4-3 Calculation Method of Carbon Nanorings

We applied PBE and hybrid B3LYP functionals and imported atomic orbitals using the LANL2DZ basis set to find the geometrical orientation and electronic properties of the N-Link and O-Link glycoprotein molecules near CNRs [43-44]. The UV-Vis spectra were calculated in the TD-DFT framework. All the calculations were performed using the Gaussian 98 package [45]. The density of states (DOS) and UV-Visible diagrams for the investigated CNRs were obtained using GussSumm software [46].

Data availability

All data generated or analysed during this study are included in this published article and its supplementary information files.

References:

[1] Naresh, V. and Lee, N., 2021. A review on biosensors and recent development of nanostructured materials-enabled biosensors. *Sensors*, *21*(4), p.1109.

[2] Meier, J., Stapleton, J., Hofferber, E., Haworth, A., Kachman, S. and Iverson, N.M., 2021. Quantification of Nitric Oxide Concentration Using Single-Walled Carbon Nanotube Sensors. Nanomaterials 2021, 11, 243.

[3] Goldt, A.E., Zaremba, O.T., Bulavskiy, M.O., Fedorov, F.S., Larionov, K.V., Tsapenko, A.P., Popov, Z.I., Sorokin, P., Anisimov, A.S., Inani, H. and Kotakoski, J., 2021. Highly efficient bilateral doping of single-walled CNTs. *Journal of Materials Chemistry C*, *9*(13), pp.4514-4521.

[4] Wang, S., Humphreys, E.S., Chung, S.Y., Delduco, D.F., Lustig, S.R., Wang, H., Parker, K.N., Rizzo, N.W., Subramoney, S., Chiang, Y.M. and Jagota, A., 2003. Peptides with selective affinity for CNTs. *Nature materials*, *2*(3), pp.196-200.

[5] Dunakey, S.J., Coyle, B.L., Thomas, A., Xu, M., Swift, B.J. and Baneyx, F., 2019. Selective labeling and decoration of the ends and sidewalls of single-walled CNTs using mono-and bispecific solid-binding fluorescent proteins. *Bioconjugate Chemistry*, *30*(3), pp.959-965.

[6] Satishkumar, B.C., Brown, L.O., Gao, Y., Wang, C.C., Wang, H.L. and Doorn, S.K., 2007. Reversible fluorescence quenching in CNTs for biomolecular sensing. *Nature Nanotechnology*, *2*(9), pp.560-564.

[7] Pinals, R.L., Ledesma, F., Yang, D., Navarro, N., Jeong, S., Pak, J.E., Kuo, L., Chuang, Y.C., Cheng, Y.W., Sun, H.Y. and Landry, M.P., 2021. Rapid SARS-CoV-2 spike protein detection by carbon nanotube-based near-infrared nanosensors. *Nano Letters*, *21*(5), pp.2272-2280.

[8] Seo, G., Lee, G., Kim, M.J., Baek, S.H., Choi, M., Ku, K.B., Lee, C.S., Jun, S., Park, D., Kim, H.G. and Kim, S.J., 2020. Rapid detection of COVID-19 causative virus (SARS-CoV-2) in human nasopharyngeal swab specimens using field-effect transistor-based biosensor. *ACS nano*, *14*(4), pp.5135-5142.

[9] Shao, W., Shurin, M.R., Wheeler, S.E., He, X. and Star, A., 2021. Rapid detection of SARS-CoV-2 antigens using high-purity semiconducting single-walled carbon nanotube-based field-effect transistors. *ACS applied materials & interfaces*, *13*(8), pp.10321-10327.

[10] Patel, S., Srivastav, A.K., Gupta, S.K., Kumar, U., Mahapatra, S.K., Gajjar, P.N. and Banerjee, I., 2021. CNTs for rapid capturing of SARS-COV-2 virus: revealing a mechanistic aspect of binding based on computational studies. *RSC Advances*, *11*(10), pp.5785-5800.

[11] Aasi, A., Aghaei, S.M., Moore, M.D. and Panchapakesan, B., 2020. Pt-, Rh-, Ru-, and Cu-single-wall CNTs are exceptional candidates for design of anti-viral surfaces: a theoretical study. *International Journal of Molecular Sciences*, *21*(15), p.5211.

[12] Daniel, S., Rao, T.P., Rao, K.S., Rani, S.U., Naidu, G.R.K., Lee, H.Y. and Kawai, T., 2007. A review of DNA functionalized/grafted CNTs and their characterization. *Sensors and Actuators B: Chemical*, *122*(2), pp.672-682.

[13] Luong, J.H., Hrapovic, S., Wang, D., Bensebaa, F. and Simard, B., 2004. Solubilization of multiwall CNTs by 3-aminopropyltriethoxysilane towards the fabrication of electrochemical biosensors with promoted electron transfer. *Electroanalysis: An International Journal Devoted to Fundamental and Practical Aspects of Electroanalysis*, *16*(1-2), pp.132-139.

[14] Liew, K.M., Jianwei, Y. and Zhang, L.W., 2016. *Mechanical behaviors of carbon nanotubes: theoretical and numerical approaches*. William Andrew.

[15] Barone, V. and Scuseria, G.E., 2004. Theoretical study of the electronic properties of narrow single-walled CNTs: Beyond the local density approximation. The Journal of chemical physics, 121(21), pp.10376-10379.

[16] Kayang, K.W., Nyankson, E., Efavi, J.K., Apalangya, V.A., Adetunji, B.I., Gebreyesus, G., Tia, R., Abavare, E.K.K., Onwona-Agyeman, B. and Yaya, A., 2019. A comparative study of the interaction of nickel, titanium, palladium, and gold metals with single-walled CNTs: A DFT approach. Results in Physics, 12, pp.2100-2106.

[17] Dresselhaus, M.S., Dresselhaus, G., Charlier, J.C. and Hernandez, E., 2004. Electronic, thermal and mechanical properties of CNTs. *Philosophical Transactions of the Royal Society of London. Series A: Mathematical, Physical and Engineering Sciences*, *362*(1823), pp.2065-2098.

[18] Rajter, R.F., French, R.H., Ching, W.Y., Podgornik, R. and Parsegian, V.A., 2013. Chirality-dependent properties of CNTs: electronic structure, optical dispersion properties, Hamaker coefficients and van der Waals–London dispersion interactions. *RSC advances*, *3*(3), pp.823-842.

[19] Samsonidze, G.G., Saito, A.R., Jorio, D.A., Pimenta, E., Souza, F., Grüneis, F.A., Dresselhaus, D.G. and Dresselhausa, M.S., 2003. The concept of cutting lines in carbon nanotube science. *Journal of nanoscience and nanotechnology*, *3*(6), pp.431-458.

[20] Gharbavi, K. and Badehian, H., 2014. Structural and electronic properties of armchair (7, 7) CNTs using DFT. *Computational materials science*, *82*, pp.159-164.

[21] Ye, J., Shao, Q., Wang, X. and Wang, T., 2016. Effects of B, N, P and B/N, B/P pair into zigzag single-walled CNTs: a first-principle study. Chemical Physics Letters, 646, pp.95-101.

[22] Tetik, E., 2015. The electronic properties of doped single walled CNTs and carbon nanotube sensors. arXiv preprint arXiv:1501.02339.

[23] Qasemnazhand, M., Khoeini, F. and Marsusi, F., 2022. Optical response of sila-fulleranes in interaction with glycoproteins for environmental monitoring. Atomic Clusters: Theory & Experiments.

[24] Jasti, R., Bhattacharjee, J., Neaton, J.B. and Bertozzi, C.R., 2008. Synthesis, characterization, and theory of [9]-,[12]-, and [18] cycloparaphenylene: carbon

nanohoop structures. Journal of the American Chemical Society, 130(52), pp.17646-17647.

[25] Omachi, H., Nakayama, T., Takahashi, E., Segawa, Y. and Itami, K., 2013. Initiation of carbon nanotube growth by well-defined carbon nanorings. Nature chemistry, 5(7), pp.572-576.

[26] Heller, D.A., Jin, H., Martinez, B.M., Patel, D., Miller, B.M., Yeung, T.K., Jena, P.V., Höbartner, C., Ha, T., Silverman, S.K. and Strano, M.S., 2009. Multimodal optical sensing and analyte specificity using single-walled CNTs. *Nature nanotechnology*, *4*(2), pp.114-120.

[27] Qasemnazhand, M., Khoeini, F. and Marsusi, F., 2020. Fulleryne, a new member of the carbon cages family. *arXiv preprint arXiv:2003.09835*.

[28] Wang, T., Lu, J., Zhu, H., Liu, J., Lin, X., Liu, Y. and Tang, Y., 2017. The electronic properties of chiral silicon nanotubes. *Superlattices and Microstructures*, *109*, pp.457-462.

[29] Tavakol, H. and Shahabi, D., 2015. DFT, QTAIM, and NBO study of absorption of rare gases into and on the surface of sulfur-doped, single-wall CNTs. *The Journal of Physical Chemistry C*, *119*(12), pp.6502-6510.

[30] Zhan, C.G., Nichols, J.A. and Dixon, D.A., 2003. Ionization potential, electron affinity, electronegativity, hardness, and electron excitation energy: molecular properties from density functional theory orbital energies. *The Journal of Physical Chemistry A*, *107*(20), pp.4184-4195.

[31] Marsusi, F. and Qasemnazhand, M., 2016. Sila-fulleranes: promising chemically active fullerene analogs. *Nanotechnology*, *27*(27), p.275704.

[32] Ireta, J., Neugebauer, J. and Scheffler, M., 2004. On the accuracy of DFT for describing hydrogen bonds: dependence on the bond directionality. *The Journal of Physical Chemistry A*, *108*(26), pp.5692-5698.

[33] Grimme, S., Antony, J., Ehrlich, S. and Krieg, H., 2010. A consistent and accurate ab initio parametrization of density functional dispersion correction (DFT-D) for the 94 elements H-Pu. *The Journal of chemical physics*, *132*(15), p.154104.

[34] Qasemnazhand, M., Khoeini, F. and Marsusi, F., 2021. Optical response of sila-fulleranes in interaction with glycoproteins for environmental monitoring. *Frontiers in Physics*, p.340.

[35] Giannozzi, P., Andreussi, O., Brumme, T., Bunau, O., Nardelli, M.B., Calandra, M., Car, R., Cavazzoni, C., Ceresoli, D., Cococcioni, M. and Colonna, N., 2017. Advanced capabilities for materials modelling with Quantum ESPRESSO. *Journal of physics: Condensed matter*, *29*(46), p.465901.

[36] Giannozzi, P., Baroni, S., Bonini, N., Calandra, M., Car, R., Cavazzoni, C., Ceresoli, D., Chiarotti, G.L., Cococcioni, M., Dabo, I. and Dal Corso, A., 2009. QUANTUM ESPRESSO: a modular and open-source software project for quantum simulations of materials. *Journal of physics: Condensed matter*, *21*(39), p.395502.

[37] Monkhorst, H.J. and Pack, J.D., 1976. Special points for Brillouin-zone integrations. *Physical review B*, *13*(12), p.5188.

[38] Dass, D. and Vaid, R., 2018. Chirality dependence of electronic band structure and density of states in single-walled CNTs. *The African Review of Physics*, *12*.

[39] Wilder, J.W., Venema, L.C., Rinzler, A.G., Smalley, R.E. and Dekker, C., 1998. Electronic structure of atomically resolved CNTs. *Nature*, *391*(6662), pp.59-62.

[40] Dass, D. and Vaid, R., 2018. Chirality dependence of electronic band structure and density of states in single-walled CNTs. *The African Review of Physics*, *12*.

[41] 中西毅, 1999. R. Saito, G. Dresselhaus and MS Dresselhaus, Physical Properties of Carbon Nanotubes, Imperial College Press, London, 1998, xii+ 259p., 22× 15.5 cm,\10,560 [学部・大学院向, 専門書]. *日本物理学会誌*, *54*(10), pp.832-833.

[42] Samsonidze, G.G., Saito, A.R., Jorio, D.A., Pimenta, E., Souza, F., Grüneis, F.A., Dresselhaus, D.G. and Dresselhausa, M.S., 2003. The concept of cutting lines in carbon nanotube science. *Journal of nanoscience and nanotechnology*, *3*(6), pp.431-458.

[43] Chiodo, S., Russo, N. and Sicilia, E., 2006. LANL2DZ basis sets recontracted in the framework of density functional theory. *The Journal of chemical physics*, *125*(10), p.104107.

[44] Qasemnazhand, M., Khoeini, F. and Marsusi, F., 2021. Predicting the new carbon nanocages, fullerynes: a DFT study. *Scientific reports*, *11*(1), pp.1-14.

[45] Petersson, G.A., Malick, D.K., Wilson, W.G., Ochterski, J.W., Montgomery Jr, J.A. and Frisch, M.J., 1998. Calibration and comparison of the Gaussian-2, complete basis set, and density functional methods for computational thermochemistry. *The Journal of chemical physics*, *109*(24), pp.10570-10579.

[46] O'boyle, N.M., Tenderholt, A.L. and Langner, K.M., 2008. Cclib: a library for package-independent computational chemistry algorithms. Journal of computational chemistry, 29(5), pp.839-845.

Supplementary Files

This is a list of supplementary files associated with this preprint. Click to download.

- supplementaryinformation.docx